RESEARCH ARTICLE

Brain
Pathology

Downregulated GPR30 expression in the epileptogenic foci of female patients with focal cortical dysplasia type IIb and tuberous sclerosis complex is correlated with 18F-FDG PET-CT values

Zhongke Wang[1] | Kaixuan Huang[1] | Xiaolin Yang[1] | Kaifeng Shen[1] | Ling Yang[2] |
Ruotong Ruan[3] | Xianjun Shi[1] | Miao Wang[1] | Gang Zhu[1] | Meihua Yang[1] |
Chunqing Zhang[1] | Shengqing Lv[1] | Hui Yang[1] | Xiaotang Fan[2] | Shiyong Liu[1]

[1]Epilepsy Research Center of PLA, Department of Neurosurgery, Xinqiao Hospital, Army Medical University (Third Military Medical University), Chongqing, China

[2]Department of Developmental Neuropsychology, School of Psychology, Army Medical University (Third Military Medical University), Chongqing, China

[3]Department of Basic Medical College, Army Medical University (Third Military Medical University), Chongqing, China

Correspondence
Shiyong Liu, Epilepsy Research Center of PLA, Department of Neurosurgery, Xinqiao Hospital, Army Medical University, No. 183 Xinqiao Main Street, Shapingba District, Chongqing 400037, China.
Email: liushi24252016@163.com

Xiaotang Fan, Department of Developmental Neuropsychology, School of Psychology, Army Medical University (Third Military Medical University), Chongqing, China.
Email: fanxiaotang2005@163.com

Abstract

Focal cortical dysplasia type IIb (FCDIIb) and tuberous sclerosis complex (TSC) are typical causes of developmental delay and refractory epilepsy. G-protein-coupled receptor 30 (GPR30) is a specific estrogen receptor that is critical in neurodevelopment, neuroinflammation, and neuronal excitability, suggesting that it plays a potential role in the epilepsy of patients with FCDIIb and TSC. Therefore, we investigated the role of GPR30 in patients with FCDIIb and TSC. We found that the expression of GPR30 and its downstream protein kinase A (PKA) pathway were decreased and negatively correlated with seizure frequency in female patients with FCDIIb and TSC, but not in male patients. GPR30 was widely distributed in neurons, astrocytes, and microglia, and its downregulation was especially notable in microglia. The GPR30 agonist G-1 increased the expression of PKA and p-PKA in cultured cortical neurons, and the GPR30 antagonist G-15 exhibited the opposite effects of G-1. The NF-κB signaling pathway was also activated in the specimens of female patients with FCDIIb and TSC, and was regulated by G-1 and G-15 in cultured cortical neurons. We also found that GPR30 regulated cortical neuronal excitability by altering the frequency of spontaneous excitatory postsynaptic currents and the expression of NR2A/B. Further, the relationship between GPR30 and glycometabolism was evaluated by analyzing the correlations between GPR30 and 18F-FDG PET-CT values (standardized uptake values, SUVs). Positive correlations between GPR30 and SUVs were found in female patients, but not in male patients. Intriguingly, GPR30 expression and SUVs were significantly decreased in the epileptogenic tubers of female TSC patients, and ROC curves indicated that SUVs could predict the localization of epileptogenic tubers. Taken together, our results suggest a potential protective effect of GPR30 in the epileptogenesis of female patients with FCDIIb and TSC.

1 | INTRODUCTION

Malformations of cortical development (MCDs) are the major cause of refractory epilepsy (1,2). MCDs are a group of severe brain malformations associated with intractable epilepsy, intellectual disability, cognitive impairment, and autism spectrum disorders (3,4). Focal cortical dysplasia IIb (FCDIIb) and tuberous sclerosis complex (TSC) are typical MCDs with similar pathological characteristics, such as dysmorphic neurons (DNs), bright eosinophilic giant cells (GCs), and balloon cells (BCs) (4–6). Resected brain tissues of patients with FCDIIb and TSC exhibit increased expression of glutamate transporters, NMDA receptors, and proinflammatory factors. Increased neuronal excitability and activated inflammation ultimately lead to epileptogenesis in patients with FCDIIb and TSC (7–9). However, the detailed molecular mechanisms underlying the epilepsy of patients with FCDIIb and TSC remain unclear.

Estrogen is a crucial regulator of neurodevelopment, neuronal excitability, and neuroinflammation in the central nervous system (CNS) (10–12). Clinical evidence and animal experiments have shown that estrogen has a proconvulsant effect (13,14). Estrogen acts through nuclear receptors (estrogen receptor [ER]α and ERβ) and G protein-coupled receptor 30 (GPR30). ERα and ERβ mediate the genomic effects of estrogen (15), and ERα has been reported to increase seizure susceptibility (14,16). GPR30 is a membrane receptor that regulates the non-genomic effects of estrogen, including calcium mobilization, kinase activation, and nitric oxide production (17–19). It is reported to be two to four times more abundant than ERα or ERβ in the rat prefrontal cortex and binds estradiol with a higher affinity than ERα and ERβ (19,20). Moreover, GPR30 is selectively activated by the 17α and 17β isomers of estradiol, but does not bind other steroids, including progesterone, testosterone, or cortisol. GPR30 has been reported to regulate neuronal excitability in myelinated vagal afferent neurons and reduce the release of TNF-α, IL-1β, and IL-6 in microglia (21,22), but the role of GPR30 in the epileptogenesis of patients with FCDIIb and TSC is still unknown.

To explore the role of GPR30 in the epilepsy of patients with FCDIIb and TSC, we detected the expression and distribution of GPR30, analyzed the correlation between GPR30 expression and clinical variables, and explored the expression of the downstream PKA signaling pathway. In addition, we also explored GPR30-mediated NF-κB inflammatory signaling and cortical neuronal excitability. Furthermore, the correlation between GPR30 and ^{18}F-FDG PET-CT standardized uptake values (SUVs) was analyzed in patients with FCDIIb and TSC, and the potential predictive value of SUVs on epileptogenic tubers was assessed in female patients with TSC.

2 | MATERIALS AND METHODS

2.1 | Human subjects

Eighty-two human subjects comprising patients with FCDIIb (n = 30), TSC (n = 30), and control individuals (n = 22) were obtained from the Department of Neurosurgery at Xinqiao Hospital (Army Medical University, Chongqing, China). All procedures were performed according to the guidelines of the Declaration of Helsinki of the World Medical Association and the Ethics Committee guidelines of Army Medical University. Patients underwent comprehensive presurgical evaluation and signed informed consent for the use of resected brain tissues in research and access to medical records before the surgery. All surgical specimens were reviewed by two neuropathologists based on the International League Against Epilepsy classification (23). Additional clinical mutation analyses of TSC 1 and TSC 2 were performed to confirm the diagnosis of TSC. The control specimens were from 22 autopsies of individuals without a known neurologic or psychiatric history. According to our previous studies (24), all the specimens were collected within 6 h after death because most proteins are stable in this postmortem interval (25). All control cases were assessed by two neuropathologists and were diagnosed as histologically normal. The menstruation of females was recorded, and specimens from females with menstruation were collected within three days after menstruation to avoid estrogen fluctuation.

2.2 | Tissue preparation

Human specimens were divided into representative tissue blocks during surgery. One part of the tissue block was fixed in 10 % buffered formalin for 24–48 h, embedded in paraffin, and used for standard histopathologic diagnosis, pathologic classification, immunohistochemistry, and immunofluorescence. Another part of the tissue block was immediately frozen in

liquid nitrogen, stored at −80°C, and used for quantitative real-time polymerase chain reaction and western blot analyses.

2.3 | Quantitative real-time polymerase chain reaction (qRT-PCR)

Total RNA was extracted from the FCDIIb, TSC, and control specimens using TRIzol (Invitrogen, Carlsbad, CA, USA) according to the manufacturer's instructions. The concentration and purity of the RNA were determined using a spectrophotometer (Ocean Optics, Dunedin, FL, USA) at 260/280 nm, and then total RNA was reverse-transcribed to cDNA. Total cDNA was synthesized using 1 μg of total RNA and an oligo (dT) primer (TaKaRa, Otsu, Japan). PCR primers were designed based on the complementary DNA sequence. The primers used in this study were as follows: GPR30 (forward: AGTCTTTCCGTCACGCCTACC; reverse: GGCTCGTCTTCTGCTCCACA), IL-1β (forward: ATGATGGCTTATTACAGTGGCAA; reverse: GTCGGAG ATTCGTAGCTGGA), IL-6 (forward: ACTCACCTCTT CAGAACGAATTG; reverse: CCATCTTTGGAAGGTT CAGGTTG), and TNF-α (forward: CCTCTCTCTAATC AGCCCTCTG; reverse: GAGGACCTGGGAGTAGAT GAG). GAPDH served as the endogenous control gene for normalization. The PCR amplification conditions were as follows: 95°C for 30 s (7), 95°C for 5 s (40 cycles), and 60°C for 30 s (1 cycle). Finally, the quantitative analyses of the data were calculated according to the $2^{-\Delta\Delta CT}$ method.

2.4 | Immunohistochemistry (IHC) and immunofluorescence (IF)

Paraffin-embedded tissues were sectioned at 5 μm, deparaffinized in xylene, rehydrated through graded alcohol, and heated for 25 min by boiling citrate buffer (pH 6.0) for antigen retrieval in a microwave oven. Sections were incubated in 0.5% H_2O_2 for 30 min at 37°C to quench endogenous peroxidase and then incubated in 3% bovine serum albumin (BSA) for 1 h at 4°C to block nonspecific binding. Next, the sections were incubated with primary antibodies overnight at room temperature. The primary antibodies used in this study were as follows: anti-GPR30 (1:400, Abcam, England), anti-NeuN (1:500; Millipore, Billerica, MA, USA), anti-GFAP (glial fibrillary acidic protein) (1:500; Sigma, England), anti-CD68 (1:400; Abcam, England), and anti-Iba1 (1:1000, Wako, Japan). BSA was used instead of primary antibodies in the negative controls. After the sections were washed, they were incubated with the corresponding secondary antibodies at 1:200 dilutions for 2 h at room temperature, and subsequently incubated with the avidin-biotin-peroxidase complex for 2 h at 37°C and 3,3-diaminobenzidine tetrahydrochloride (DAB, Boster, China) to stain the target protein. Counterstaining was performed with hematoxylin. For IF, sections were incubated with the corresponding Cy3- or 488-conjugated secondary antibodies (both at 1:500, Jackson ImmunoResearch, West Grove, PA, USA) for 2 h at 37°C, and mounted with Vectashield (Vector). Nuclei were subsequently stained with 4′,6-diamidino-2-phenylindole (DAPI, Beyotime, China). The stained sections were photographed with a Zeiss Axio Vert microscope (Zeiss, Oberkochen, Germany) equipped with a Zeiss Axiocam digital color camera connected to the Zeiss AxioVision 3.0 system.

2.5 | Evaluation of immunostaining and cell counting

The intensity of GPR30, PKA, p-PKA, and NF-κB in DNs and BCs were evaluated as previously described (26) with a semi-quantitative scale ranging from 0 to 3 (0: -, no; 1: ±, weak; 2: +, moderate; 3: ++, strong immunoreactivity). The frequency scores of GPR30, PKA, p-PKA, and NF-κB positive cells [(i) single to 10%; (ii) 11–50%; (iii) >50%] were also analyzed to evaluate the relative number of positive cells within the specimens of patients. The product of these two values (intensity and frequency scores) was taken to give the immunoreactivity score. Mean optical density (MOD) of GPR30 was examined according to a previous report (27). Briefly, stained sections were assessed at 400× magnification using an Olympus BX63 microscope (Olympus, Shinjuku-ku, Tokyo, Japan). The captured images were analyzed using Image-Pro Plus software (IPP) (Media Cybernetics, Bethesda, MD, USA), and the MOD was measured. In addition, we calculated the labeling index (LI) of double-labeled and the percentage of Iba1-positive cells in FCDIIb and TSC tissues. The LI was defined as the ratio of labeled cells relative to the entire cell population of selected fields. Two blinded investigators evaluated the specific immunoreactivity and LI, and the overall concordance was >90%.

2.6 | Primary cells isolation and protein extraction

Primary cortical neurons were isolated from E18.5 C57/B6 mouse embryos. Briefly, cortical tissues from the brains of the mouse embryos were digested with 0.05 % trypsin-EDTA.Na$_2$ at 37°C for 12 min and dissociated cortical cells were plated at a density of 1×10^5 on poly D-lysine-coated 24-well plates in Planting Medium (DMEM-H medium with 10 % [vol/vol] FBS, 1 % [vol/vol] GlutaMAX, and 1 % [vol/vol] penicillin–streptomycin). After 4 h, cells were cultured in Neuron Medium (Neurobasal medium containing 1/50 [vol/vol] B27 and 1 % [vol/vol] GlutaMAX) for another 14 days for screening and maturation in a humidified 5 % CO_2 incubator at 37°C.

To determine the signaling pathways of GPR30, cultured cortical neurons were treated with DMSO, GPR30 agonist (G-1, Cayman Chemical Company, USA) (1 μM), or GPR30 antagonist (G-15, Cayman Chemical Company, USA) (1 μM) for 1 h for 14 days. After the treatments, cultures were washed with cold PBS (pH 7.2), lysed in cold lysis buffer (N-PER, Thermo Scientific, MA), and then harvested with a cell scraper, followed by centrifugation at 12,000 rpm for 10 min. Protein concentrations were determined using the BCA Assay (Pierce Biotechnology, IL).

2.7 | Ovariectomized (OVX) mice model

Female C57/B6 mice were used in this study. All experiments were performed in accordance with the Guide for the Care and Use of Laboratory Animals (Guide) (NRC 2011) and approved by the Animal Studies Committee of the Army Medical University. Mice were housed in a temperature-controlled room with an alternately light-dark cycle (12 h/12 h) and could access standard food and water ad libitum. All mice in underwent bilateral ovariectomy at 3 weeks old as described previously (28). Mice were anesthetized using 1.5% isoflurane, and both the left and right ovaries were removed. After surgery, mice were allowed to recover for 1 week. To maintain estrogen concentration at the physiological level, all mice were injected with β-estradiol (10 mg/kg, i.p.) per day after recovery until they were sacrificed.

2.8 | Whole-cell patch-clamp recording

Five-week-old female mice were decapitated to prepare brain slices according to previously described methods (29). Briefly, mice were sacrificed, and their brains were dissected rapidly. Horizontal brain slices (300 μm) were cut (Leica VT1200S; Nussloch, Germany) in the slice solution (4°C) (2 mM CaCl2, 2 mM MgCl2, 2.5 mM KCl, 26 mM NaHCO3, 1.25 mM KH2PO4, 10 mM glucose, and 220 mM sucrose [pH 7.4] continuously bubbled with 95% O2/5% CO2). Then, the brain slices were transferred to the ACSF (37°C) (126 NaCl, 26 NaHCO3, 10 glucose, 3 KCl, 1.4 NaH2PO4, 2 CaCl2, and 1 MgCl2 mM continuously bubbled with 95% O2/5% CO2). The pH of the ACSF was adjusted to 7.35–7.40 with HCl or NaOH, and the osmolarity was adjusted to 300–305 mOsm with double distilled water. Borosilicate glass capillaries were fabricated using a horizontal puller (P-97, Sutter Instruments, Inc.) to give a resistance of 3–6 MΩ when filled with intracellular solution. For whole-cell patch-clamp recordings, the brain slices were initially perfused in flowing ACSF containing KA (1 μM) (4 ml/min) to establish an in vitro epilepsy model. Then, the GPR30 agonist G-1 (10 μM) and antagonist G-15 (10 μM) were added to the perfusate.

For spontaneous excitatory postsynaptic current (sEPSC) recording, glass electrodes were filled with the following internal solution (in mM): 120 potassium methane-sulfonate, 10 NaCl, 10 EGTA, 1 CaCl2, 10 HEPES, 5 ATP-Mg, pH adjusted to 7.2 with KOH, with an osmolarity of 300 mOsm. For spontaneous inhibitory postsynaptic currents (sIPSC) recording, glass electrodes were filled with the following internal solution (in mM): 130 cesium methane-sulfonate, 10 sodium methanesulfonate, 10 EGTA, 1 CaCl2, 10 HEPES, 5 lidocaine N-ethyl bromide quaternary salt-Cl, 2 ATP-Mg, pH adjusted to 7.2 with CsOH, with an osmolarity of 300 mOsm. All recordings were performed at a holding membrane potential of −70 mv and at room temperature. Signals from the cortex of mice were acquired using a MultiClamp 700B amplifier (Axon, USA) and recorded using pClamp 9.2 software (Molecular Devices, Sunnyvale, CA, USA). The signals were filtered at 5 kHz, digitized at 20 kHz, and analyzed with Clampfit 10.0 software and Mini Analysis Program (Synaptosoft, Leonia, NJ, USA).

2.9 | Western blot analysis

Total protein was extracted from human specimens and cultured cortical neurons using a whole protein extraction kit (Beyotime Institute of Biotechnology, Jiangsu, China); protein content was measured using a BCA protein assay (Bio-Rad, Hercules, CA, USA). The protein was mixed with a 5 × loading buffer and subjected to electrophoresis. Equal amounts of protein (30 mg/lane) were separated on a 10 % sodium dodecyl sulfate-polyacrylamide gel and transferred onto polyvinylidene fluoride membranes (Millipore, Billerica, MA, USA) using a wet electroblotting system (Bio-Rad, Hercules, CA, USA). Membranes were blocked in blocking buffer at room temperature for 2 h and then incubated overnight at 4°C with primary antibodies against GPR30 (1:1000, Abcam, England), protein kinase A (PKA) C-α (1:1000; Cell Signaling Technology, USA), phosphorylated PKA (p-PKA) C (Thr197) (1:1000; Cell Signaling Technology, USA), NF-κB (1:500, Cell Signaling Technology, USA), and GAPDH (1:1000; Cell Signaling Technology, USA). After three washes in Tris-buffered saline containing 0.5 % Tween-20, the samples were labeled with peroxidase-conjugated goat anti-rabbit secondary antibody (1:1000; Zhongshan Goldenbridge Biotechnology Co., Beijing, China) for 1 h at room temperature. Specific protein bands on the membranes were visualized using enhanced chemiluminescence, and densitometry was performed with Image-Pro Plus software (Media Cybernetics, Silver Spring, MD). Glyceraldehyde 3-phosphate dehydrogenase (GAPDH) levels were evaluated as a loading control.

2.10 | ^{18}F-FDG PET-CT imaging

Previous studies have shown that ^{18}F-FDG PET/CT, which combines molecular and structural imaging, can be successfully used as a presurgical workup for patients with FCDIIb and TSC (30,31). PET-CT scans were performed according to the guidelines issued by the Chinese Society of Nuclear Medicine. The criteria are summarized as follows: at least 4 h of fasting before scanning, blood glucose levels below 11.1 mmol/L, and PET acquisitions 1 h after the injection of 3 MBq/kg of FDG. PET examination was performed using a Biograph 64 True Point PET/CT scanner and a Discovery ST system. Attenuation correction was performed using CT. The CT comprised a 64-slice multidetector-row spiral scanner with a transverse field of view of 700 mm and displayed the registered images on a workstation. Static images were reconstructed using an iterative 3D method with a Gaussian filter (6 mm FWHM) (pixel size = 2.0×2.0 mm with a slice thickness of 1.5 mm). Patients were in an awake, resting state, and head movements were monitored carefully during scanning. No patients had clinical seizure activity after the injection of FDG or during the PET/CT scan. Two experienced nuclear medicine physicians evaluated the PET images independently and confirmed the hypometabolic regions. The data and the MRI images of the patients were confirmed by the two physicians to ensure the disease focus. PET/CT was analyzed with a previously validated semiautomatic approach by exploiting 3D Slicer™ (32). In brief, the hypometabolic foci of the patient images were segmented, and the segmented foci were output as regions of interest (ROIs). PET standardized uptake value modules were performed in the 3D Slicer, and the maximum and mean standardized uptake values (SUVmax, SUVmean) of the ROIs were computed. Finally, the results were output to a comma-separated value (csv) file for further analysis.

2.11 | Statistical analysis

The analysis was carried out using a one-way analysis of variance (ANOVA) among the FCDIIb, TSC, and control groups. Differences in sex, age, epilepsy duration, and seizure frequency were assessed using t-tests. For bivariate correlation analyses, we used Spearman's rank correlation test. For patch-clamp recordings, 11 cells were analyzed for each condition investigated. The effects of G-1 and G-15 were normalized to the KA-induced steady baseline and analyzed using the paired t-test. To determine whether PET could predict epileptogenic tubers in female patients with TSC, we calculated a receiver operating characteristic (ROC) curve, and the area under the curve (AUC) was compared with the values obtained by chance (AUC = 0.5). Significance was set at $p < 0.05$. The data are expressed as the mean ± SEM, and analysis was performed using the SPSS 18.0 package (SPSS, Inc., Chicago, IL, USA).

3 | RESULTS

3.1 | Clinical characteristics of the human subjects

The mean age of the patients with FCDIIb was 16.60 ± 1.61 years (range, 4–35 years), with 15 males and 15 females (9 of them had a menstrual history); the mean age of the TSC patients was 12.42 ± 1.50 years (range, 0.5–36 years), with 12 males and 18 females (10 of them had a menstrual history); and the mean age of the controls was 17.59 ± 3.07 years (range, 2–57 years), with 10 males and 12 females (5 of them had a menstrual history). No significant differences in sex or age were found in the FCDIIb, TSC, and control subjects ($p > 0.05$). There were also no significant differences in sex ($p = 0.440$), age ($p = 0.062$), epilepsy duration ($p = 0.211$), and seizure frequency ($p = 0.54$) between the patients with FCDIIb and those with TSC. The clinical features of all human subjects are summarized in Table 1. The detailed features of the specimens from the control subjects are shown in Table 2. In addition, IHC was used to reconfirm the presence of DNs and BCs in specimens of patients with FCDIIb and TSC. Consistent with previous studies (33), there was no immunoreactivity for GFAP and Vimentin, but consistent immunoreactivity for SMI32 in the DNs.

TABLE 1 Summary of the clinical features of FCDIIb, TSC patients, and controls

Variable	Control (n = 22)	FCD IIb (n = 30)	TSC (n = 30)	*p* value
Gender ratio (M/F)	10/12	15/15	12/18	>0.05
Age (year)	17.59 ± 3.07	16.60 ± 1.61	12.42 ± 1.50	>0.05
Range	2–57	4–35	0.5–36	
Epilepsy duration (year)	NA	3.63 ± 1.81	2.98 ± 2.15	>0.05
Range	NA	1–8	0.2–7	
Seizure frequency (month)	NA	50.63 ± 22.58	47.13 ± 21.36	>0.05
Range	NA	21–106	13–105	

Abbreviations: F, female; FCD, focal cortical dysplasia; M, male; TSC, tuberous sclerosis complex.

Case No.	Gender	Age (year)	Cause of death	PMI (h)	Diagnosis	Seizure
1	F	16	Liver rupture	2.0	Normal	None
2	M	21	Aortoclasia	0.5	Normal	None
3	M	7	Congenital heart disease	1.0	Normal	None
4	M	16	Splenic rupture	2.2	Normal	None
5	F	5	Congenital heart disease	1.6	Normal	None
6	F	57	Myocardial infarction	2.1	Normal	None
7	M	22	Aortoclasia	0.7	Normal	None
8	M	8	Cardiac arrest	2.0	Normal	None
9	F	7	Pneumonia	1.8	Normal	None
10	F	32	Splenic rupture	1.4	Normal	None
11	M	2	Heart failure	1.0	Normal	None
12	F	16	Heart failure	0.5	Normal	None
13	M	41	Hemopneumothorax	4.0	Normal	None
14	F	12	Pneumonia	2.0	Normal	None
15	F	43	Splenic rupture	3.5	Normal	None
16	M	6	Respiratory failure	0.5	Normal	None
17	M	20	Hemopneumothorax	2.5	Normal	None
18	F	2	Congenital heart disease	0.5	Normal	None
19	F	5	Cardiac arrest	3.0	Normal	None
20	F	17	Respiratory failure	2.5	Normal	None
21	F	10	Heart failure	3.0	Normal	None
22	M	22	Splenic rupture	2.5	Normal	None

Abbreviations: F, female; M, male; PMI, post-mortem interval (interval between death of a patient and removal of the brain before freezing or fixation).

And variable immunoreactivity for GFAP, Vimentin, and SMI32 was observed in the BCs (black arrows) (Figure S1A–F).

Molecular analysis of TSC cortical tubers is shown in Table 3. Twenty-eight non-mosaic mutations were identified in the 30 patients with TSC. There were twenty-two unique small mutations, and one of which (TSC2-exon 15, 1513C > T) was seen twice in these samples with small mutations. These small mutations included four deletion mutations, eight insertion mutations, and ten single base substitution mutations. Among all mutations detected in this study, ten mutations had been reported previously in TSC patients, while 13 mutations were unreported previously. In addition, there was one patient who had genomic deletions of Exons 21–23 within the TSC1 gene, and four patients had genomic deletions of various sizes within the TSC2 gene.

3.2 | Expression of GPR30 in patients with FCDIIb and TSC

The RNA and protein levels of GPR30 were examined in surgical specimens from the FCDIIb, TSC, and control groups. For specimens from male patients, there were no significant differences in the RNA levels (Figure 1A;

FCDIIb: $p = 0.296$, TSC: $p = 0.643$) and protein levels (Figure 1C,D; FCDIIb: $p = 0.389$, TSC: $p = 0.609$) of GPR30 compared with controls. However, in the specimens from female patients, significantly decreased GPR30 RNA and protein levels were detected in the FCDIIb (RNA: $p < 0.05$; protein: $p < 0.01$) and TSC groups (RNA and protein both $p < 0.01$) compared with controls (Figure 1B,E,F). Next, the correlations between GPR30 expression and different clinical variables (age at surgery, epilepsy duration, and seizure frequency) of female patients were assessed. There were significant inverse correlations between GPR30 expression and seizure frequency in female patients with FCDIIb ($r = −0.6366$, $p = 0.0107$; Figure 1G) and TSC ($r = −0.6100$, $p = 0.0072$; Figure 1H). However, no significant correlations were found between GPR30 expression and age at surgery and epilepsy duration in female patients (data not shown).

3.3 | Distribution of GPR30 in the specimens from female patients with FCDIIb and TSC

The distribution of GPR30 in specimens from female patients and controls was evaluated by IHC and IF. GPR30 expression was found in both DNs

TABLE 3 Non-mosaic mutations identified in TSC brain tubers from 30 female TSC patients

| Exon	Mutation	Type; effect on protein	Previously reported (R) or not (NR)	Sanger sequencing result
TSC1-exon 5	338delT	Frameshift	R	Heterozygpus
TSC1-exon 10	989_990insT	Frameshift	NR	Heterozygpus
TSC1-exon 15	1888_1891delAAAG	Frameshift	NR	Heterozygpus
TSC1-exon 18	2304_2305insT	Frameshift	NR	Heterozygpus
TSC2-exon 8	689_690insCCTGC	Frameshift	NR	Heterozygpus
TSC2-exon 14	1372C > T	R458X	NR	Heterozygpus
TSC2-exon 15	1513C > T (2)	R505X	R	Heterozygpus
TSC2-exon 16	1600-2A > C	Splice	NR	Heterozygpus
TSC2-exon 17	1827_1828insA	Frameshift	NR	Heterozygpus
TSC2-exon 18	1947-2A > G	Splice	R	Heterozygpus
TSC2-exon 18	1975_1976insC	Frameshift	NR	Heterozygpus
TSC2-exon 20	2130_2131del insA	Frameshift	NR	Heterozygpus
TSC2-exon 27	3094C > T	R1032X	R	Heterozygpus
TSC2-exon 27	3201_3202insA	Frameshift	NR	Heterozygpus
TSC2-exon 27	3204_3205delTG	Frameshift	R	Heterozygpus
TSC2-exon 30	3412C > T	R1138X	R	Heterozygpus
TSC2-exon 31	3751A > T	K1251X	NR	Heterozygpus
TSC2-exon 34	4183C > T	Q1395X	R	Heterozygpus
TSC2-exon 34	4355C > T	S1452L	R	Heterozygpus
TSC2-exon 35	4494-1G > A	Splice	R	Heterozygpus
TSC2-exon 37	4682_4683insC	Frameshift	NR	Heterozygpus
TSC2-exon 42	5419_5420insT	Frameshift	NR	Heterozygpus
TSC1 big del	Exons 21-23	Deletion	R	N/A
TSC2 big del	Exons 1-16	Deletion	NR	N/A
TSC2 big del	Exons 21-23	Deletion	R	N/A
TSC2 big del	Exons 32-42	Deletion	R	N/A
TSC2 big del	Exons 39-42	Deletion	R	N/A

Abbreviations: N/A, not applicable; TSC, tuberous sclerosis complex.

and BCs (Figure 2B,C and Figure S2A,E). There were 74.6 ± 9% of DNs and 77.2 ± 5.4% of BCs showed GPR30 staining in female patients with FCDIIb, and there were 75.7 ± 8.4% of DNs and 71.8 ± 9% of BCs showed GPR30 staining in female patients with TSC (Figure S2I,J). In addition, the MOD of GPR30 was decreased in female patients compared with controls (Figure 2A–D; FCDIIb: $p < 0.01$, TSC: $p < 0.01$). IF revealed that GPR30 was widely distributed in the neurons (Figure 2E–G), astrocytes (Figure 2I–K), and microglia (Figure 2M–O) of female patients and controls. The LI was calculated and revealed that GPR30 expression was significantly decreased in the microglia (Figure 2H,L,P; FCDIIb: $p < 0.05$, TSC: $p < 0.05$).

3.4 | Expression of PKA signaling pathway in female patients with FCDIIb and TSC

IHC was used to evaluate the immunostaining of GPR30 downstream PKA signaling pathways in the specimens of female patients with FCDIIb (Figure S2B,C) and TSC (Figure S2F,G). PKA staining were observed in DNs (76.9 ± 6.7% in FCDIIb, 69.7 ± 7.3% in TSC) and BCs (78.3 ± 5.7% in FCDIIb, 70.2 ± 5.7% in TSC). And p-PKA immunoreactivity were also observed in DNs (67.2 ± 5.2% in FCDIIb, 63.7 ± 6.4% in TSC) and BCs (64.3 ± 7% in FCDIIb, 61.2 ± 9.4% in TSC) (Figure S2I,J). Furthermore, quantitative analysis of PKA signaling pathways was performed using western blots. The expression of PKA and p-PKA was decreased in FCDIIb (PKA: $p < 0.01$; p-PKA: $p < 0.01$) and TSC (PKA: $p < 0.01$; p-PKA: $p < 0.01$) compared with controls (Figure 3A–C). In addition, GPR30 expression was positively correlated with the expression of PKA and p-PKA in FCDIIb (PKA: r = 0.6339, $p = 0.0112$; p-PKA: r = 0.5511, $p = 0.0332$) and TSC (PKA: r = 0.4835, $p = 0.0421$; p-PKA: r = 0.5967, $p = 0.0089$) (Figure 3D,E). We found that seizure frequency was negatively correlated with PKA and p-PKA expression in FCDIIb (PKA: r = −0.6324, $p = 0.0114$; p-PKA: r = −0.6729, $p = 0.0060$) and TSC (PKA: r = −0.5659, $p = 0.0144$; p-PKA: r = −0.5858, $p = 0.0106$) (Figure 3F,G).
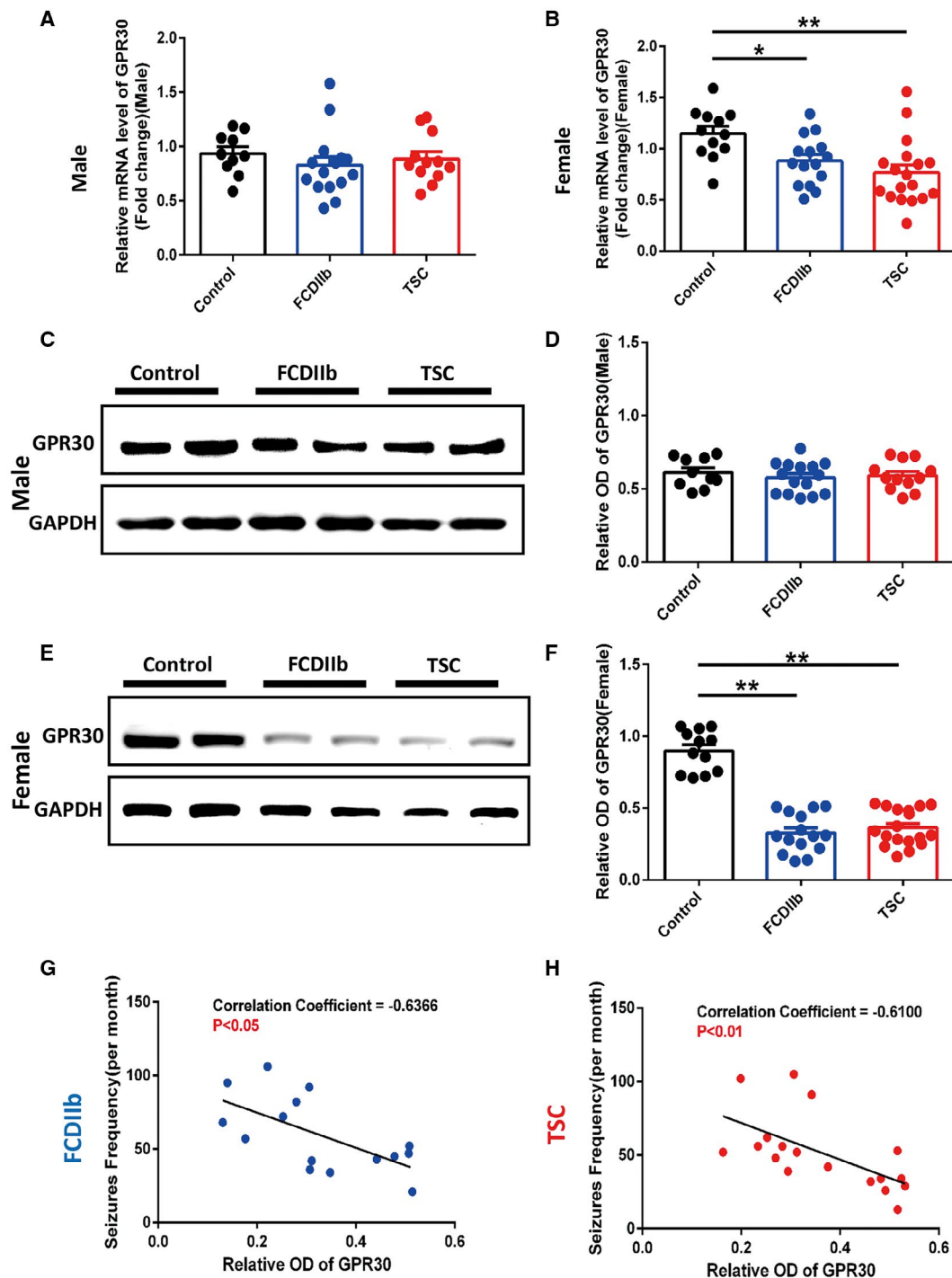
FIGURE 1 The expression of GPR30 in the FCDIIb, TSC, and control groups. (A, B) GPR30 RNA levels in the patients and the controls were measured by RT-PCR. (C-F) Representative immunoblot bands and densitometric analysis show the protein level of GPR30. There were no significant differences in the male patients and the controls; however, significant downregulation of GPR30 was detected in female patients with FCDIIb and TSC. The data are expressed as the mean ± SEM, *$p < 0.05$, **$p < 0.01$. (G, H) Correlations between GPR30 and seizure frequency in female patients with FCDIIb and TSC. The scatter plot shows a significant negative correlation in female patients with FCDIIb ($r = -0.6366$, $p = 0.0107$) and TSC ($r = -0.6100$, $p = 0.0072$) [Colour figure can be viewed at wileyonlinelibrary.com]

3.5 | Inflammation in female patients with FCDIIb and TSC

GPR30 expression was significantly decreased in microglia, and GPR30 was reported to rescue neuroinflammation. Next, we explored the expression of microglia and the activation of the NF-κB-mediated inflammatory pathway in female patients with FCDIIb and TSC. IF revealed significantly more Iba1-positive microglia in FCDIIb ($p < 0.01$) and TSC ($p < 0.05$) than
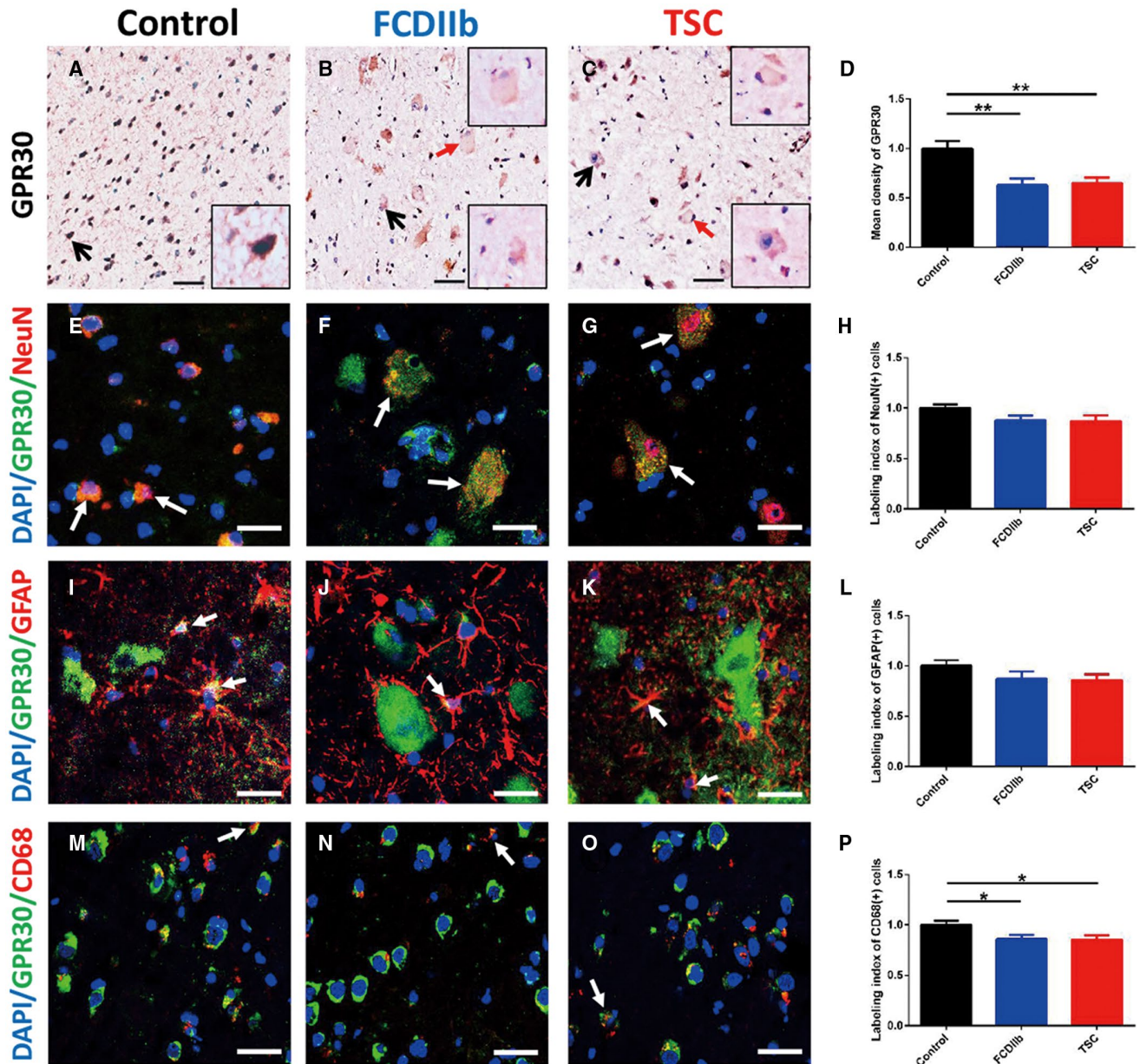
FIGURE 2 Distribution of GPR30 in female patients with FCDIIb, TSC, and female controls. (A-C) IHC of GPR30 in the surgical samples. A high mean density of GPR30 was detected in the neurons of the controls (arrows in A), and a low mean density was detected in the relatively normal neurons (black arrows) and the aberrant neurons (BCs) (red arrows) of the FCDIIb (B) and TSC groups (C). Scale bar = 50 μm. (D) Mean density of GPR30. The mean density was decreased in the FCDIIb and TSC groups compared to that in the control group. (E-O) IF staining shows the distribution of GPR30 in the neurons, astrocytes, and microglia. (E-G): Colocalization of GPR30 with NeuN in neurons; (I-K) colocalization of GPR30 with GFAP in astrocytes; (M-O) colocalization of GPR30 with CD68 in microglia. Scale bar = 25 μm. (H, L, P) Labeling index (LI) of GPR30 in neurons, astrocytes, and microglia. GPR30 was primarily decreased in the microglia of female patients. The data are expressed as the mean ± SEM, *$p < 0.05$, **$p < 0.01$ [Colour figure can be viewed at wileyonlinelibrary.com]

in controls (Figure 4A–D). IHC showed both DNs and BCs were immunoreactive for NF-κB (Figure S2D,H). There were 69.3 ± 11% of DNs and 72.4 ± 8.2% of BCs showed NF-κB staining in female patients with FCDIIb, and 74.1 ± 6.8% of DNs and 69.2 ± 8.7% of BCs showed NF-κB staining in female patients with TSC (Figure S2I,J). Besides, NF-κB pathway was activated in female patients compared with controls (Figure 4E,F; FCDIIb: $p < 0.01$, TSC: $p < 0.01$). RNA levels of the inflammatory

factors IL-1β (FCDIIb: $p < 0.05$, TSC: $p < 0.05$), IL-6 (FCDIIb: $p < 0.01$, TSC: $p < 0.01$), and TNF-α (FCDIIb: $p < 0.01$, TSC: $p < 0.05$), which are regulated by NF-κB, were also increased in female patients (Figure 4G). The correlation between NF-κB and GPR30 expression and seizure frequency was evaluated, and we found that NF-κB expression was negatively correlated with GPR30 expression and positively correlated with seizure frequency (data not shown).
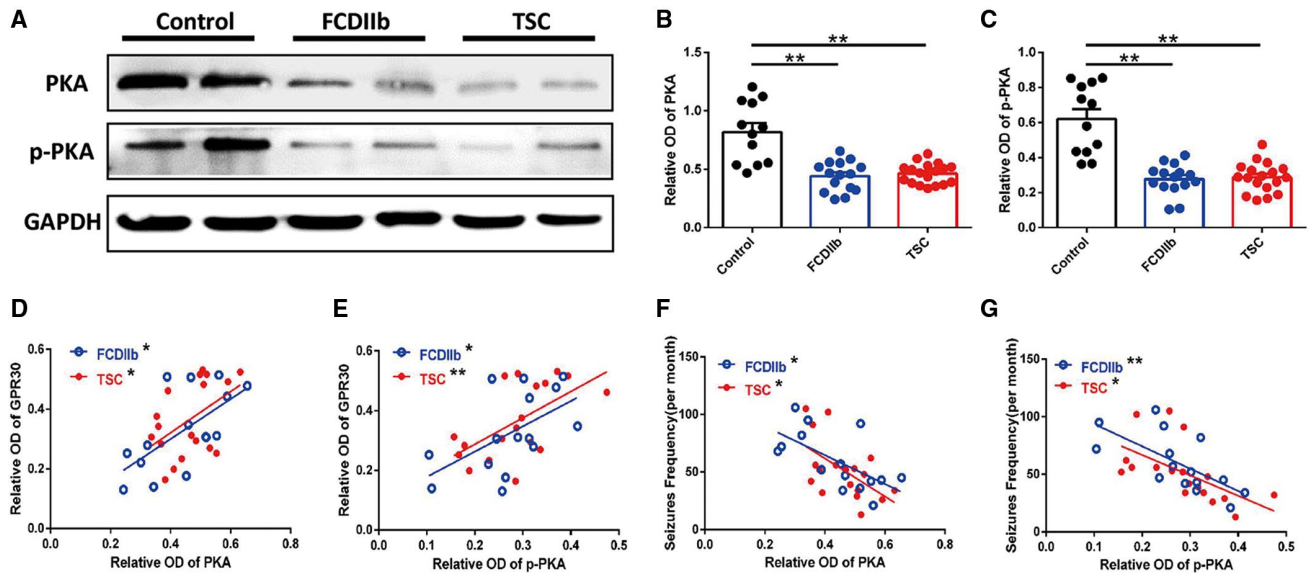
FIGURE 3 Altered expression of the PKA signaling pathway in female patients. (A) Western blot of PKA and phosphorylated PKA (p-PKA) in the surgical samples. (B, C) Statistical analysis shows that the PKA and p-PKA protein levels are decreased in female patients with FCDIIb and TSC. The data are expressed as the mean ± SEM, **$p < 0.01$. (D) Correlation of PKA with GPR30. The protein level of PKA was significantly positively correlated with GPR30 in female patients with FCDIIb ($r = 0.6339$, $p = 0.0112$) and TSC ($r = 0.4835$, $p = 0.0421$). (E) Correlation between p-PKA and GPR30. The expression of p-PKA was positively correlated with GPR30 in female patients with FCDIIb ($r = 0.5511$, $p = 0.0332$) and TSC ($r = 0.5967$, $p = 0.0089$). (F) Correlation between PKA and seizure frequency. The protein level of PKA was significantly negatively correlated with seizure frequency in female patients with FCDIIb ($r = -0.6324$, $p = 0.0114$) and TSC ($r = -0.5659$, $p = 0.0144$). (G) Correlation between p-PKA and seizure frequency. The protein level of p-PKA was significantly negatively correlated with seizure frequency in female patients with FCDIIb ($r = -0.6729$, $p = 0.0060$) and TSC ($r = -0.5858$, $p = 0.0106$) [Colour figure can be viewed at wileyonlinelibrary.com]

3.6 | Effects of G-1 and G-15 on the GPR30 Signaling Pathways

GPR30 regulation of the PKA and NF-κB signaling pathways was detected in cultured cortical neurons after treatment with DMSO, G-1 (1 μM), or G-15 (1 μM) (Figure 5A). G-1 treatment increased the expression of PKA ($p < 0.05$) and p-PKA ($p < 0.01$), whereas G-15 treatment decreased the expression of PKA ($p < 0.05$) and p-PKA ($p < 0.01$) (Figure 5B). In addition, NF-κB expression was decreased in cortical neurons treated with G-1 ($p < 0.05$), and increased in cortical neurons treated with G-15 ($p < 0.01$) (Figure 5B). These results suggest that GPR30 regulates the PKA and NF-κB signaling pathways.

3.7 | Role of GPR30 in cortical neuronal excitability

To explore the role of GPR30 in cortical neuronal excitability, we evaluated the sEPSCs (Figure 6A) and sIPSCs (Figure 6D) of cortical neurons treated with G-1 or G-15 in our in vitro epileptic model. The sEPSC frequency was decreased after G-1 treatment ($p < 0.01$) and increased after G-15 treatment ($p < 0.05$) (Figure 6B) in the in vitro epileptic model, but the sEPSC amplitude was not affected by either G-1 or G-15 treatment (Figure 6C). Both

the frequency and amplitude of sIPSCs were not affected by G-1 or G-15 treatment (Figure 6E,F) in the in vitro epileptic model. These results indicate that GPR30 regulates excitatory synaptic transmission. Therefore, we detected the expression of NR2A and NR2B in cultured cortical neurons treated with G-1 or G-15 (Figure 6G). G-1 treatment decreased the expression of both NR2A ($p < 0.01$) and NR2B ($p < 0.01$), whereas G-15 treatment increased the expression of both NR2A ($p < 0.01$) and NR2B ($p < 0.05$) (Figure 6H,I).

3.8 | Correlation between GPR30 and the SUVs in Patients with FCDIIb and TSC

^{18}F-FDG PET-CT can reflect glycometabolism by the maximum and mean standardized uptake values (SUVmax and SUVmean), and GPR30 has been reported to regulate glycometabolism. The SUVs were assessed by 3D Slicer software to reflect the glucose metabolism of female patients with FCDIIb and TSC (Figure 7A,F). We found that the SUVs were positively correlated with GPR30 expression in female patients with FCDIIb (Figure 7B,C; SUVmax: $r = 0.5782$, $p = 0.0240$, SUVmean: $r = 0.6296$, $p = 0.0119$) and TSC (Figure 7G,H; SUVmax: $r = 0.5683$, $p = 0.0139$, SUVmean: $r = 0.5513$ $p = 0.0177$). Female patients who had significantly increased premenstrual seizure frequency were further
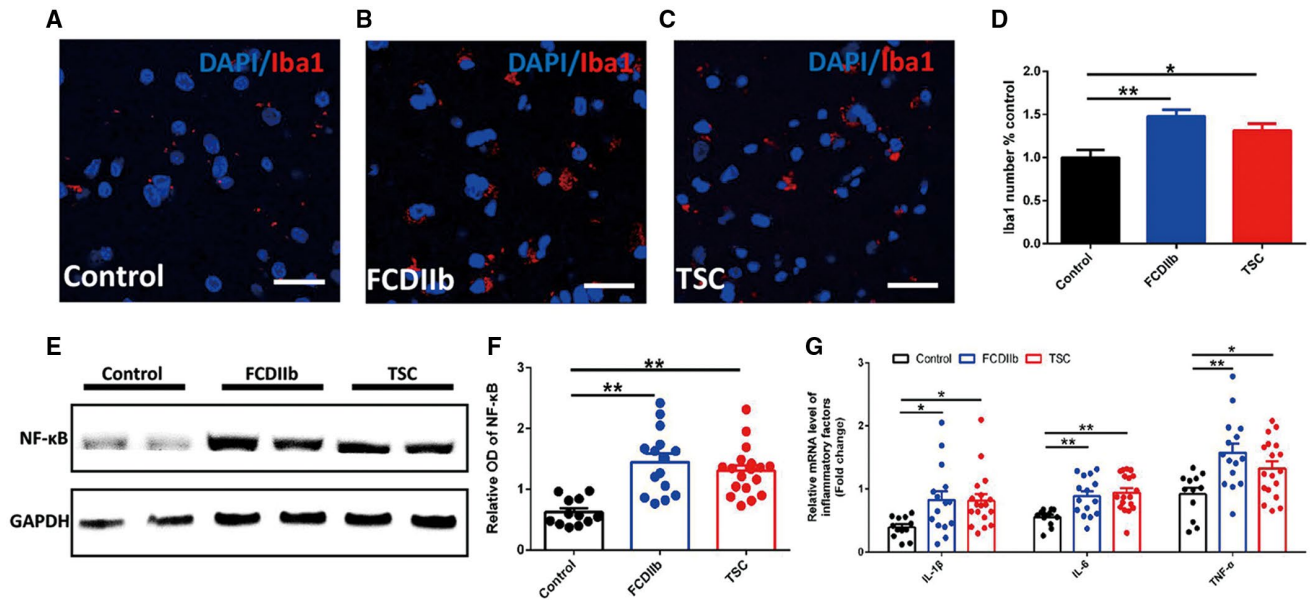
FIGURE 4 Activation of inflammation in female specimens. (A-C) IF staining shows Iba1-positive microglia. Scale bar = 25 μm. (D) Percentage of Iba1-positive cells. There were more Iba1-positive cells in the FCDIIb and TSC groups than in the control group. (E, F) Representative immunoblot bands and densitometric analysis of total homogenates of the patient and control tissues. The NF-κB protein levels were significantly increased in female patients with FCDIIb and TSC. (G) RT-PCR of inflammatory factors in the surgical specimens. Compared with those in the controls, IL-1β, IL-6, and TNF-α were significantly increased in female patients with FCDIIb and TSC. The data are expressed as the mean ± SEM, *$p < 0.05$, **$p < 0.01$ [Colour figure can be viewed at wileyonlinelibrary.com]
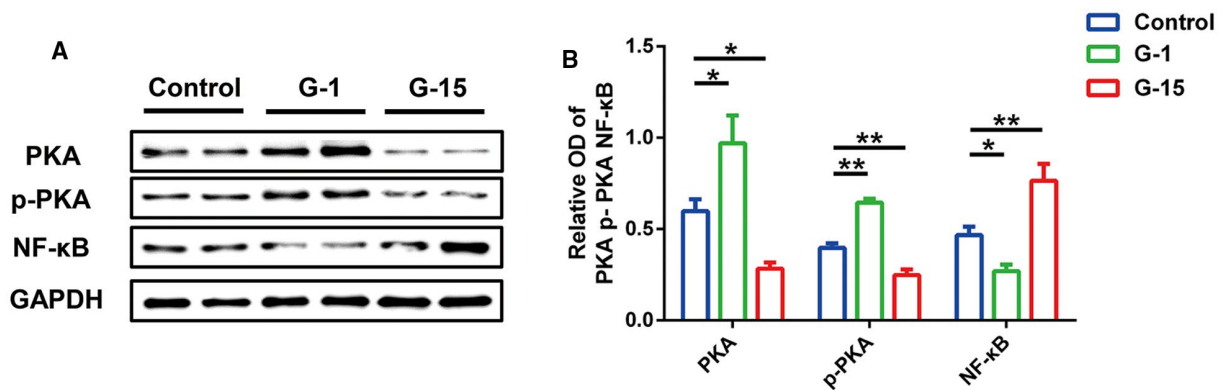
FIGURE 5 G-1- and G-15-regulation of GPR30 and the downstream PKA and NF-κB signaling pathways. (A) Western blot of PKA, p-PKA, and NF-κB in the primary cortical neurons treated with DMSO, G-1, or G-15. (B) Statistical data of the expression of PKA, p-PKA, and NF-κB. G-1 treatment increased the expression of PKA and p-PKA, and decreased the expression of NF-κB. G-15 treatment did the opposite. The data are expressed as the mean ± SEM, *$p < 0.05$, **$p < 0.01$ [Colour figure can be viewed at wileyonlinelibrary.com]

selected, and we found a strong positive correlation between GPR30 expression and SUVs in those with FCDIIb (Figure 7D,E; SUVmax: $r = 0.8787$, $p = 0.0092$, SUVmean: $r = 0.9144$, $p = 0.0039$) and TSC (Figure 7I,J; SUVmax: $r = 0.8861$, $p = 0.0079$, SUVmean: $r = 0.8832$, $p = 0.0084$). In contrast, we found no significant correlation between the SUVs and GPR30 in all patients and in male patients with FCDIIb (Figure S3A–E; all patients: SUVmax: $r = 0.3123$, $p = 0.1373$, SUVmean: $r = 0.3059$ $p = 0.1461$; male patients: SUVmax: $r = 0.2898$, $p = 0.4494$, SUVmean: $r = 0.04364$ $p = 0.9112$) and TSC (Figure S3F–J; all patients: SUVmax: $r = 0.3033$,

$p = 0.1321$; SUVmean: $r = 0.1752$, $p = 0.3921$; male patients: SUVmax: $r = −0.6096$, $p = 0.1086$; SUVmean: $r = −0.2652$, $p = 0.5255$).

3.9 | Expression and correlation of GPR30 and the SUVs in the epileptogenic tubers of female patients with TSC

The epileptogenic tubers were defined according to our previous study (34). Some prominent non-epileptogenic tubers that were >3–4 cm, had a nidus of calcification,
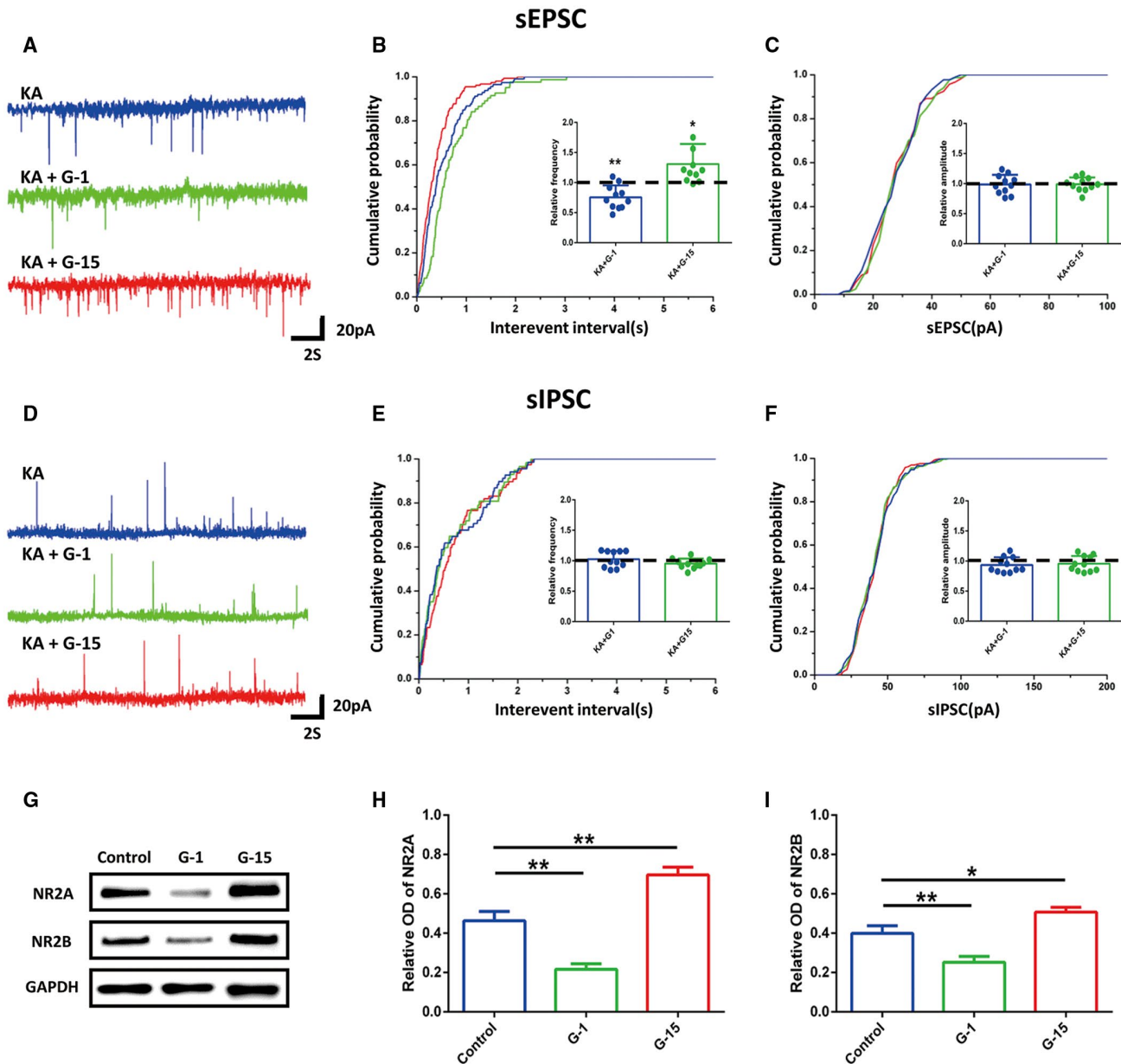
FIGURE 6 Effects of GPR30 on the regulation of cortical neuronal excitability. (A) Typical traces of sEPSCs in cells treated with KA, G-1, or G-15. (B, C) The cumulative probability for interevent intervals and amplitude of sEPSC. G-1 and G-15 treatment decreased and increased the frequency, respectively. There were no significant changes in the amplitude of sEPSC. (D) Typical traces of sIPSCs in cells treated with KA, G-1, or G-15. (E, F) The cumulative probability for interevent intervals and amplitude of sIPSC. Neither G-1 nor G-15 treatment affected the frequency and amplitude of sIPSCs. (G) Protein levels of NR2A and NR2B in the primary cortical neurons treated with DMSO, G-1, or G-15. (H, I) Densitometric analysis of NR2A and NR2B. G-1 treatment decreased the expression of NR2A and NR2B, and G-15 treatment increased the level of NR2A and NR2B in cultured cortical neurons. The data are expressed as the mean ± SEM, *$p < 0.05$, **$p < 0.01$ [Colour figure can be viewed at wileyonlinelibrary.com]

and located in the nonfunctional brain areas within the operative fields, were resected due to their potential to develop into epileptogenic tubers. We assayed the GPR30 protein levels in epileptogenic tubers (n = 11) and non-epileptogenic tubers (n = 13) obtained from female patients with TSC by western blotting and found that GPR30 expression was significantly decreased in epileptogenic tubers (Figure 8A,B; $p < 0.05$). In addition, GPR30 expression was positively correlated with SUVs in the epileptogenic tubers (Figure 8C,D; SUVmax:

r = 0.6246, $p = 0.0399$; SUVmean: r = 0.6646, $p = 0.0257$), but not in the non-epileptogenic tubers (Figure S4A,B; SUVmax: r = 0.3633, $p = 0.2225$; SUVmean: r = 0.4130, $p = 0.1607$). Notably, epileptogenic tubers had decreased SUVs (n = 11) (Figure 8E–G; SUVmax: $p < 0.01$; SUVmean: $p < 0.05$) compared with non-epileptogenic tubers (n = 30). The ROC curve demonstrated that both SUVmax (Figure 8H, AUC = 0.855 ± 0.061, $p = 0.001$) and SUVmean (Figure 8I, AUC = 0.755 ± 0.085, $p = 0.013$) could predict the location of epileptogenic tubers, and
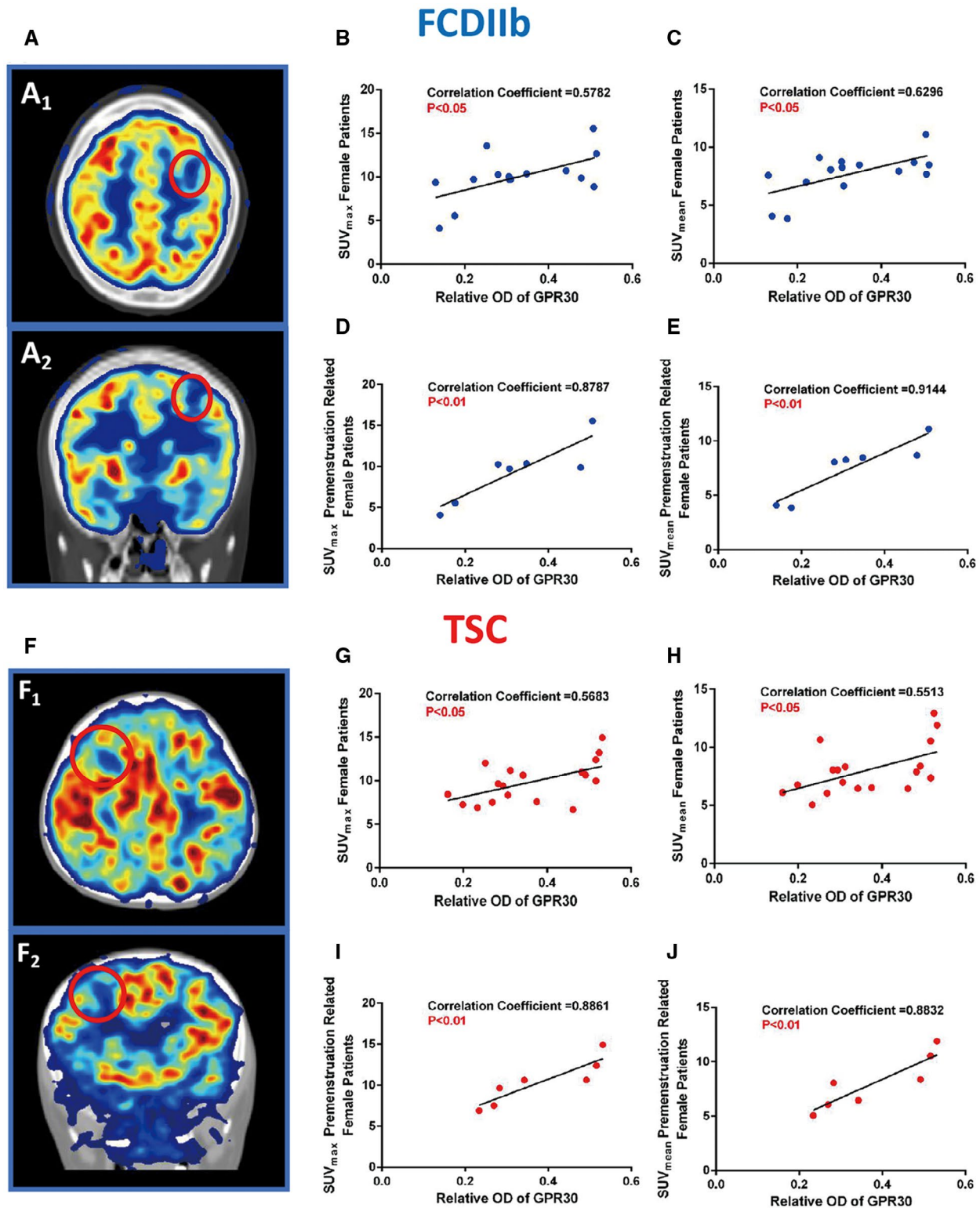
FIGURE 7 Positive correlation between GPR30 expression and SUVs in female patients with FCDIIb and TSC. (A) The axial (A_1) and coronal (A_2) PET-CT images of female patients with FCDIIb. Red circles were used to mark the epileptogenic foci of patients with FCDIIb. (B, C) Correlation of GPR30 expression with the SUVs (SUVmax and SUVmean) in female patients with FCDIIb. SUVmax and SUVmean were positively correlated with the expression of GPR30 ($r = 0.5782$, $p = 0.0240$; $r = 0.6296$ $p = 0.0119$). (D, E) Correlation of GPR30 expression with the SUVs in female FCDIIb patients with a high premenstrual epilepsy frequency. GPR30 expression was significantly positively correlated with SUVmax and SUVmean ($r = 0.8787$, $p = 0.0092$; $r = 0.9144$, $p = 0.0039$). (F) The axial (F_1) and coronal (F_2) PET-CT images of female patients with TSC. Red circles were used to mark the epileptogenic foci of patients with TSC. (G, H) Correlation of GPR30 with the SUVs in female patients with TSC. SUVmax and SUVmean were positively correlated with the expression of GPR30 ($r = 0.5683$, $p = 0.0139$; $r = 0.5513$ $p = 0.0177$). (I, J) Correlation of GPR30 with the SUVs in female TSC patients with a high premenstrual epilepsy frequency. SUVmax and SUVmean were positively correlated with the expression of GPR30 ($r = 0.8861$, $p = 0.0079$; $r = 0.8832$, $p = 0.0084$) [Colour figure can be viewed at wileyonlinelibrary.com]

that SUVmax was a better predictor than SUVmean. Therefore, SUVs could be used as a marker to predict epileptogenic tubers.

4 | DISCUSSION

In this study, we discovered that the expression of GPR30 and the activity of its downstream PKA signaling pathway were decreased and negatively correlated with seizure frequency in female patients with FCDIIb and TSC, but not in male patients. We found that GPR30 was widely distributed in the CNS and its expression was significantly reduced in microglia of female patients with FCDIIb and TSC. Moreover, the NF-κB-mediated inflammatory signaling pathway was activated in female patients and cultured cortical neurons treated with G-15. Next, we found that GPR30 regulated cortical neuronal excitability in an in vitro epileptic model by affecting sEPSC frequency and NR2A/B expression. Further, GPR30 expression was positively correlated with SUVs in female patients with FCDIIb and TSC, but not in male patients. Notably, both GPR30 expression

and SUVs were decreased in the epileptogenic tubers of female patients with TSC, and SUVs could be used to locate the epileptogenic tubers. These findings suggest that GPR30 might have an anti-epileptogenic effect in female patients with FCDIIb and TSC and provided a potential treatment target for female patients with epilepsy.

4.1 | GPR30 and epileptogenesis

Estrogen has been shown to have proconvulsant properties in both human and animal models (13,35). This phenomenon is particularly demonstrated in catamenial epilepsy; seizure activity in female patients with catamenial epilepsy has been linked to fluctuating estrogen levels and the ratio of serum estradiol/progesterone levels during the menstrual cycle (13). Estrogen acts through its receptors (ERα, ERβ, and GPR30) (15). A previous study has shown that ERα regulates the genomic effects of estrogen, increasing neuronal excitability by suppressing estradiol-induced IPSCs in the CA1 region of the hippocampus and promoting epileptogenesis (35). In contrast to ERα, GPR30 regulates non-genomic responses
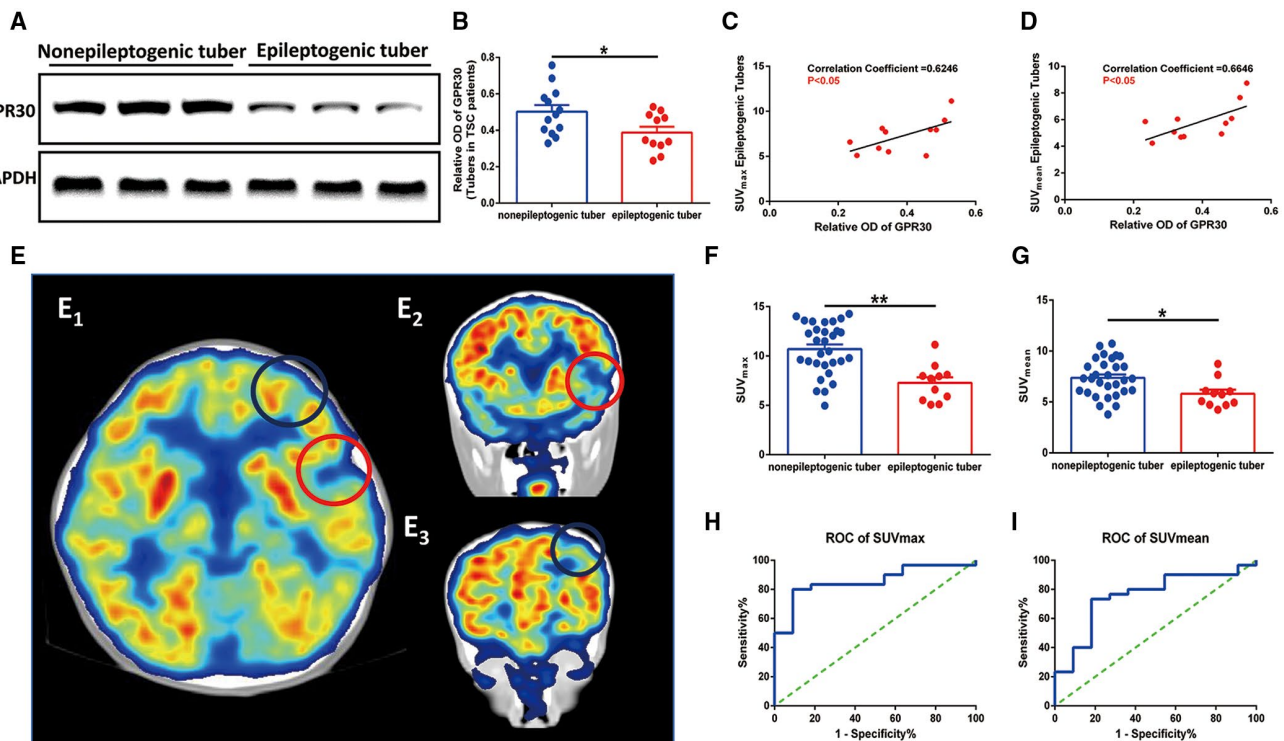
FIGURE 8 Decreased expression and positive correlation between GPR30 and SUVs in the epileptogenic tubers of female TSC patients. (A) The protein levels of GPR30 in non-epileptogenic and epileptogenic tubers. (B) Densitometric analysis of GPR30. The expression of GPR30 was decreased in the epileptogenic tubers. The data are expressed as the mean ± SEM, *$p < 0.05$, **$p < 0.01$. (C, D) Spearman's rank correlation test of GPR30 and SUVs in the epileptogenic tubers. GPR30 expression was positively correlated with SUVmax (r = 0.6246, $p = 0.0399$) and SUVmean (r = 0.6646, $p = 0.0257$) in the epileptogenic tubers. (E) The axial (E_1) and coronal PET-CT images of the epileptogenic (E_2) and non-epileptogenic (E_3) tubers were derived from the same female patients with TSC. Red circles were used to mark the epileptogenic tubers, and blue circles were used to mark the nonepileptogenic tubers. (F, G) SUVmax and SUVmean of the epileptogenic and non-epileptogenic tubers. The SUVs were reduced in the epileptogenic tubers compared to the non-epileptogenic tubers. (H, I) ROCs for the SUVs from the epileptogenic and non-epileptogenic tubers. The curve indicated that SUVmax and SUVmean predicted the epileptogenic tubers (SUVmax: AUC = 0.855 ± 0.061, $p = 0.001$; SUVmean: AUC = 0.755 ± 0.085, $p = 0.013$) [Colour figure can be viewed at wileyonlinelibrary.com]

that occur in a time frame of seconds to minutes and has a higher affinity for estrogen (20). GPR30 can mediate protective effects in neuronal excitability, regulate the excitatory/inhibitory balance in the myelinated vagal afferents, and attenuate glutamate neurotoxicity by depressing the phosphorylation of NR2B-containing NMDARs (21,36–38). In the current study, we found that the expression of GPR30 and its downstream PKA pathway was decreased and negatively correlated with seizure frequency in female patients with FCDIIb and TSC, but not in male patients. Moreover, GPR30 expression was decreased in the epileptogenic tubers of female patients with TSC compared to non-epileptogenic tubers. Treatment with G-1 decreased the frequency of sEPSC in an in vitro epileptic model and the expression of NR2A and NR2B in cultured cortical neurons; however, G-15 showed the opposite effects of G-1. These results indicated that GPR30 might participate in the epileptogenesis of female patients with FCDIIb and TSC.

Although both ERα and GPR30 are ligands of estrogen, their roles are quite different. Many studies have reported the antagonistic effects of GPR30 and ERα. High expression of GPR30 has been shown to inhibit ERα expression by attenuating PKA signaling and damage to ERα-dependent uterine growth (39). Moreover, ERα has been shown to antagonize the GPR30-mediated effects in the hippocampus, and estradiol downregulates GPR30 via an ERα-dependent mechanism (20). Therefore, GPR30 downregulation may disrupt the balance between GPR30 and ERα leading to epileptogenesis in female patients with FCDIIb and TSC. In addition, although an ERα inhibitor could be used to antagonize the epileptogenesis of female patients, it could also affect the normal functions of estrogen and produce many side effects. In contrast, GPR30 may have potential antiepileptic effects and could recover estrogen function by selective activation; therefore, GPR30 may be a better treatment target than ERα to antagonize epileptogenesis in female patients with FCDIIb and TSC.

The PKA pathway can be activated directly by GPR30 and exerts neuroprotective and anticonvulsant effects (40). Activation of the PKA pathway is necessary for the regulation of neuronal excitability, the long-lasting forms of synaptic plasticity and the upregulation of $GABA_A$-R in cerebellar interneurons, hippocampal dentate granule cells, and CA1 pyramidal neurons (41–43). In this study, we found that the expression of both PKA and p-PKA was decreased, positively correlated with GPR30 expression, and negatively correlated with seizure frequency in female patients with FCDIIb and TSC. In addition, G-1 treatment increased the expression of PKA and p-PKA, and G-15 had the opposite effects, in cultured mouse cortical neurons. These findings indicate that GPR30 might modulate the epileptogenesis of female patients with FCDIIb and TSC through the PKA pathway.

In addition, GPR30 regulates neurodevelopment, protects against the neurodegeneration of hippocampal neurons (44) and is significantly upregulated in the developing forebrain and midbrain of groupers (45). The PKA pathway has also been reported to regulate hippocampal neurogenesis, alleviate neuronal apoptosis, and attenuate cognitive impairment in epileptic rats (46–48). Therefore, the reduced expression of GPR30 and PKA may increase epilepsy susceptibility by affecting neurodevelopment and neuronal differentiation in female patients with FCDIIb and TSC.

4.2 | GPR30 and inflammation

Neuroinflammation could contribute to neuronal hyperexcitability in the seizure onset areas, and previous studies have confirmed that neuroinflammation induces epileptogenesis in patients with FCDIIb and TSC (7). Activation of microglia, release of inflammatory cytokines, and abnormalities of Toll-like receptors have been shown in the resected brain tissue of patients with FCDIIb and TSC (7,49,50). GPR30 has been reported to reduce the release of TNF-α, IL-1β, and IL-6 in microglia by inhibiting TLR4 protein expression and NF-κB activity (22,51). In vivo and in vitro experiments have indicated that G1 inhibits the generation of lipopolysaccharide-induced cytokines in human and murine macrophages (51). The GPR30 downstream PKA signaling pathway has been reported to promote microglial polarization to the M2a type, and inhibition of the cAMP-PKA pathway has been shown to lead to an increase in the hippocampal neuronal inflammatory response (52,53). In this study, we found that GPR30 expression was significantly reduced in microglia and that the NF-κB signaling pathway and its downstream inflammatory cytokines (IL-1β, IL-6, and TNF-α) were upregulated in the specimens of female patients compared with controls. Furthermore, a negative correlation between NF-κB and GPR30 expression was found in the specimens of female patients, and NF-κB expression could be regulated by both G-1 and G-15 treatment in cultured cortical neurons. These results suggest that GPR30 can modulate inflammation during the epileptogenesis of female patients with FCDIIb and TSC.

4.3 | GPR30 and ^{18}F-FDG PET-CT

^{18}F-FDG PET reflects glycometabolism by SUVs, and ER expression can affect ^{18}F-FDG-PET SUVs. Upregulation of ERs has been shown to increase ^{18}F-FDG SUV in uterine sarcoma; in contrast, ER downregulation results in a high SUVmax in breast cancer (54,55). GPR30 has been reported to regulate glucose metabolism and is expressed in most islet endocrine cells, and deletion of GPR30 impairs glucose tolerance (56,57). Previous studies have also shown that the activation of PKA signaling can upregulate glucose intake

(58,59). These findings suggest that GPR30 may affect PET SUVs. In this study, we found that GPR30 was positively correlated with SUVs in female patients. This result indicates that decreased expression of GPR30 may cause glucose hypometabolism and facilitate epileptogenesis. PET may serve as a marker to predict the expression of GPR30 in female patients with FCDIIb and TSC. Some female patients had a high seizure frequency and more severe seizures during menstruation. In these female patients, estrogen levels play a major role in epileptogenesis and glycometabolism. Intriguingly, there were more obvious positive correlations between GPR30 and SUVs in these female patients. We assumed that the SUVs are more sensitive to GPR30 in estrogen-related female patients, and further studies are needed to verify our hypothesis.

Furthermore, we explored the correlation between SUVs and GPR30 in all patients and in male patients. Interestingly, there were no significant correlations in both total and male patients. Some studies have reported that the GPR30 regulation of energy metabolism is female-specific, and female mice but not male mice show glucose intolerance with age (60). Moreover, there were no changes in insulin and glucagon secretion in male GPR30 KO mice, and glucose homeostasis and the incidence of diabetes were similar to those in WT mice (61). These studies suggested that GPR30 mediated glucose metabolism mainly in females but not in males. Therefore, PET-CT could be a noninvasive tool to predict the expression of GPR30 in female patients with FCDIIb and TSC.

4.4 | GPR30 and epileptogenic tubers

Surgical intervention in refractory epilepsy of TSC patients can be challenging, because multiple tubers are found in TSC patients. Many studies have reported methods to distinguish epileptogenic and non-epileptogenic tubers, such as diffuse tensor imaging, high-resolution electroencephalogram, and PET (62,63). PET reflects glycometabolism, and GPR30 can regulate glucose metabolism in female patients. However, little is known about the role of GPR30 and PET-CT in different tubers of female patients. In the current study, we observed that GPR30 expression was decreased in the epileptogenic tubers compared with the non-epileptogenic tubers of female TSC patients, and was positively correlated with the SUVs of epileptogenic tubers. We further identified that the SUVs were reduced in the epileptogenic tubers of female patients and could predict the epileptogenic tubers. These results illustrate that GPR30 is a crucial link between epileptogenic tubers and the SUVs, and that PET can provide a noninvasive way to recognize epileptogenic tubers in female patients with TSC. However, further research including more female patients is needed to validate these findings.

5 | CONCLUSION

In summary, we found that GPR30 potentially affected epileptogenesis by modulating neuroinflammation and neuronal excitability in female patients with FCDIIb and TSC. In addition, we found that decreased GPR30 expression was positively correlated with hypo-glycometabolism in the epileptogenic foci of female patients with FCDIIb and TSC by analyzing the correlation between GPR30 and PET-CT SUVs. Intriguingly, both GPR30 expression and SUVs were decreased in the epileptogenic tubers of female TSC patients, and SUVs could be used to predict the location of epileptogenic tubers. Therefore, our results offer a potential therapeutic strategy for female patients with FCDIIb and TSC, and show that PET-CT SUVs might be a noninvasive marker to reflect GPR30 expression and the localization of epileptogenic tubers in female patients. However, there are some limitations to this study. The number of human participants in each group was barely acceptable, limiting the universality of our results. Moreover, the specific molecular indicator of PET should be synthesized to image GPR30 and confirm our results in this study.

CONFLICTS OF INTEREST
The authors have no conflicts of interest.

AUTHOR CONTRIBUTIONS
SYL, XTF, and ZKW designed the experiments. HY, SQL, and CQZ performed the study supervision. XLY, XJS, MW, MHY, and SYL contributed to collecting clinical data and the selection of tissue samples. Western blotting, IHC, and IF were performed by ZKW, KXH, XLY, RTR, and GZ. ZKW and LY were involved in the experiments in vitro. ZKW, XLY, and KFS carried out the whole-cell patch-clamp recording. ZKW and XLY finished the statistical analysis. ZKW wrote the first draft and was responsible for incorporating the revision from other authors. SYL and XTF reviewed the final draft and provided comments. All authors read and approved the final manuscript.

DATA AVAILABILITY STATEMENT
The data that support the findings of this study are available from the corresponding author upon reasonable request.

ORCID
Zhongke Wang https://orcid.org/0000-0003-2024-5841
Shiyong Liu https://orcid.org/0000-0003-2250-1693

REFERENCES

1. Barkovich AJ, Dobyns WB, Guerrini R. Malformations of cortical development and epilepsy. Cold Spring Harb Perspect Med. 2015;5(5):a022392.
2. Kuzniecky R. Epilepsy and malformations of cortical development: new developments. Curr Opin Neurol. 2015;28(2):151–7.
3. Crino PB. Focal cortical dysplasia. Semin Neurol. 2015;35(3):201–8.
4. Scholl T, Muhlebner A, Ricken G, Gruber V, Fabing A, Samueli S, et al. Impaired oligodendroglial turnover is associated with myelin pathology in focal cortical dysplasia and tuberous sclerosis complex. Brain Pathol. 2017;27(6):770–80.
5. Iyer A, Prabowo A, Anink J, Spliet WG, van Rijen PC, Aronica E. Cell injury and premature neurodegeneration in focal malformations of cortical development. Brain Pathol. 2014;24(1):1–17.
6. Muhlebner A, Iyer AM, van Scheppingen J, Anink JJ, Jansen FE, Veersema TJ, et al. Specific pattern of maturation and differentiation in the formation of cortical tubers in tuberous sclerosis omplex (TSC): evidence from layer-specific marker expression. J Neurodev Disord. 2016;8:9.
7. Arena A, Zimmer TS, van Scheppingen J, Korotkov A, Anink JJ, Muhlebner A, et al. Oxidative stress and inflammation in a spectrum of epileptogenic cortical malformations: molecular insights into their interdependence. Brain Pathol. 2019;29(3):351–65.
8. Boer K, Crino PB, Gorter JA, Nellist M, Jansen FE, Spliet WGM, et al. Gene expression analysis of tuberous sclerosis complex cortical tubers reveals increased expression of adhesion and inflammatory factors. Brain Pathol. 2009;20(4):704–19.
9. Iffland PH 2nd, Crino PB. Focal cortical dysplasia: gene mutations, cell signaling, and therapeutic implications. Annu Rev Pathol. 2017;12:547–71.
10. Azcoitia I, Barreto GE, Garcia-Segura LM. Molecular mechanisms and cellular events involved in the neuroprotective actions of estradiol. Analysis of sex differences. Front Neuroendocrinol. 2019;55:100787.
11. Duarte-Guterman P, Yagi S, Chow C, Galea LA. Hippocampal learning, memory, and neurogenesis: Effects of sex and estrogens across the lifespan in adults. Horm Behav. 2015;74:37–52.
12. Mahmoud R, Wainwright SR, Galea LA. Sex hormones and adult hippocampal neurogenesis: Regulation, implications, and potential mechanisms. Front Neuroendocrinol. 2016;41:129–52.
13. Herzog AG, Fowler KM, Sperling MR, Massaro JM. Distribution of seizures across the menstrual cycle in women with epilepsy. Epilepsia. 2015;56(5):e58–e62.
14. Scharfman HE, MacLusky NJ. Sex differences in the neurobiology of epilepsy: a preclinical perspective. Neurobiol Dis. 2014;72:180–92.
15. Eyster KM. The estrogen receptors: an overview from different perspectives. Methods Mol Biol. 2016;1366:1–10.
16. Pham DH, Tan CC, Homan CC, Kolc KL, Corbett MA, McAninch D, et al. Protocadherin 19 (PCDH19) interacts with paraspeckle protein NONO to co-regulate gene expression with estrogen receptor alpha (ERα). Hum Mol Genet. 2017;26(11):2042–52.
17. Ervin KSJ, Mulvale E, Gallagher N, Roussel V, Choleris E. Activation of the G protein-coupled estrogen receptor, but not estrogen receptor α or β, rapidly enhances social learning. Psychoneuroendocrinology. 2015;58:51–66.
18. Prossnitz ER, Arterburn JB. International Union of Basic and Clinical Pharmacology. XCVII. G protein-coupled estrogen receptor and its pharmacologic modulators. Pharmacol Rev. 2015;67(3):505–40.
19. Prossnitz ER, Arterburn JB, Smith HO, Oprea TI, Sklar LA, Hathaway HJ. Estrogen signaling through the transmembrane G protein-coupled receptor GPR30. Annu Rev Physiol. 2008;70:165–90.
20. Hadjimarkou MM, Vasudevan N. GPER1/GPR30 in the brain: Crosstalk with classical estrogen receptors and implications for behavior. J Steroid Biochem Mol Biol. 2018;176:57–64.
21. Qiao GF, Li BY, Lu YJ, Fu YL, Schild JH. 17Beta-estradiol restores excitability of a sexually dimorphic subset of myelinated vagal afferents in ovariectomized rats. Am J Physiol Cell Physiol. 2009;297(3):C654–64.
22. Zhang Z, Qin P, Deng Y, Ma Z, Guo H, Guo H, et al. The novel estrogenic receptor GPR30 alleviates ischemic injury by inhibiting TLR4-mediated microglial inflammation. J Neuroinflammation. 2018;15(1):206.
23. Blumcke I, Thom M, Aronica E, Armstrong DD, Vinters HV, Palmini A, et al. The clinicopathologic spectrum of focal cortical dysplasias: a consensus classification proposed by an ad hoc Task Force of the ILAE Diagnostic Methods Commission. Epilepsia. 2011;52(1):158–74.
24. Sun FJ, Zhang CQ, Chen X, Wei YJ, Li S, Liu SY, et al. Downregulation of CD47 and CD200 in patients with focal cortical dysplasia type IIb and tuberous sclerosis complex. J Neuroinflammation. 2016;13(1):85.
25. Hynd MR, Lewohl JM, Scott HL, Dodd PR. Biochemical and molecular studies using human autopsy brain tissue. J Neurochem. 2003;85(3):543–62.
26. Zurolo E, Iyer A, Maroso M, Carbonell C, Anink JJ, Ravizza T, et al. Activation of Toll-like receptor, RAGE and HMGB1 signalling in malformations of cortical development. Brain. 2011;134(Pt 4):1015–32.
27. Yang XL, Chen B, Zhang XQ, Chen X, Yang MH, Zhang W, et al. Upregulations of CRH and CRHR1 in the epileptogenic tissues of patients with intractable infantile spasms. CNS Neurosci Ther. 2017;23(1):57–68.
28. Ström JO, Theodorsson A, Ingberg E, Isaksson I-M, Theodorsson E. Ovariectomy and 17β-estradiol replacement in rats and mice: a visual demonstration. J Vis Exp. 2012;(64):e4013.
29. Yang Y, Tian X, Xu D, Zheng F, Lu X, Zhang Y, et al. GPR40 modulates epileptic seizure and NMDA receptor function. Sci Adv. 2018;4(10):eaau2357.
30. Desarnaud S, Mellerio C, Semah F, Laurent A, Landre E, Devaux B, et al. (18)F-FDG PET in drug-resistant epilepsy due to focal cortical dysplasia type 2: additional value of electroclinical data and coregistration with MRI. Eur J Nucl Med Mol Imaging. 2018;45(8):1449–60.
31. Liu S, Cai Y, Rong R, Hu P, Chen S, Wang X, et al. Tuberous sclerosis complex (TSC) with epilepsy on (18)F-FDG simultaneous PET/MR. Eur J Nucl Med Mol Imaging. 2020;47:2471–72.
32. Wu WJ, Li ZY, Dong S, Liu SM, Zheng L, Huang MW, et al. Texture analysis of pretreatment [(18)F]FDG PET/CT for the prognostic prediction of locally advanced salivary gland carcinoma treated with interstitial brachytherapy. EJNMMI Res. 2019;9(1):89.
33. Sugiura C, Miyata H, Ueda M, Ohama E, Vinters HV, Ohno K. Immunohistochemical expression of fibroblast growth factor (FGF)-2 in epilepsy-associated malformations of cortical development (MCDs). Neuropathology. 2008;28(4):372–81.
34. Liu S, Yu T, Guan Y, Zhang K, Ding P, Chen L, et al. Resective epilepsy surgery in tuberous sclerosis complex: a nationwide multicentre retrospective study from China. Brain. 2020;143(2):570–81.
35. Huang Guang Z, Woolley Catherine S. Estradiol acutely suppresses inhibition in the hippocampus through a sex-specific endocannabinoid and mGluR-dependent mechanism. Neuron. 2012;74(5):801–8.
36. Liu SB, Zhang N, Guo YY, Zhao R, Shi TY, Feng SF, et al. G-protein-coupled receptor 30 mediates rapid neuroprotective effects of estrogen via depression of NR2B-containing NMDA receptors. J Neurosci. 2012;32(14):4887–900.
37. Waters EM, Thompson LI, Patel P, Gonzales AD, Ye HZ, Filardo EJ, et al. G-protein-coupled estrogen receptor 1 is anatomically

positioned to modulate synaptic plasticity in the mouse hippocampus. J Neurosci. 2015;35(6):2384–97.

38. Zhang L, Ma Y, Liu M, Ma Y, Guo H. The effects of various estrogen doses on the proliferation and differentiation of cultured neural stem cells. Gen Physiol Biophys. 2019;38(5):417–25.

39. Gao F, Ma X, Ostmann AB, Das SK. GPR30 activation opposes estrogen-dependent uterine growth via inhibition of stromal ERK1/2 and estrogen receptor alpha (ERalpha) phosphorylation signals. Endocrinology. 2011;152(4):1434–47.

40. Filardo EJ, Quinn JA, Frackelton AR Jr, Bland KI. Estrogen action via the G protein-coupled receptor, GPR30: stimulation of adenylyl cyclase and cAMP-mediated attenuation of the epidermal growth factor receptor-to-MAPK signaling axis. Mol Endocrinol. 2002;16(1):70–84.

41. Lonze BE, Ginty DD. Function and regulation of CREB family transcription factors in the nervous system. Neuron. 2002;35(4):605–23.

42. Naseer MI, Shupeng L, Kim MO. Maternal epileptic seizure induced by pentylenetetrazol: apoptotic neurodegeneration and decreased GABAB1 receptor expression in prenatal rat brain. Mol Brain. 2009;2:20.

43. Zhen JL, Chang YN, Qu ZZ, Fu T, Liu JQ, Wang WP. Luteolin rescues pentylenetetrazole-induced cognitive impairment in epileptic rats by reducing oxidative stress and activating PKA/CREB/BDNF signaling. Epilepsy Behav. 2016;57(Pt A):177–84.

44. Kajta M, Rzemieniec J, Litwa E, Lason W, Lenartowicz M, Krzeptowski W, et al. The key involvement of estrogen receptor beta and G-protein-coupled receptor 30 in the neuroprotective action of daidzein. Neuroscience. 2013;238:345–60.

45. Nagarajan G, Tsai Y-J, Chen C-Y, Chang C-F. Developmental expression of genes involved in neural estrogen biosynthesis and signaling in the brain of the orange-spotted grouper Epinephelus coioides during gonadal sex differentiation. J Steroid Biochem Mol Biol. 2011;127(3–5):155–66.

46. Landeira BS, Santana T, Araujo JAM, Tabet EI, Tannous BA, Schroeder T, et al. Activity-independent effects of CREB on neuronal survival and differentiation during mouse cerebral cortex development. Cereb Cortex. 2018;28(2):538–48.

47. Min SJ, Hyun HW, Kang TC. Leptomycin B attenuates neuronal death via PKA- and PP2B-mediated ERK1/2 activation in the rat hippocampus following status epilepticus. Brain Res. 2017;1670:14–23.

48. Zhang XQ, Mu JW, Wang HB, Jolkkonen J, Liu TT, Xiao T, et al. Increased protein expression levels of pCREB, BDNF and SDF-1/CXCR4 in the hippocampus may be associated with enhanced neurogenesis induced by environmental enrichment. Mol Med Rep. 2016;14(3):2231–7.

49. Zhang B, Zou J, Han L, Beeler B, Friedman JL, Griffin E, et al. The specificity and role of microglia in epileptogenesis in mouse models of tuberous sclerosis complex. Epilepsia. 2018;59(9):1796–806.

50. Zimmer TS, Ciriminna G, Arena A, Anink JJ, Korotkov A, Jansen FE, et al. Chronic activation of anti-oxidant pathways and iron accumulation in epileptogenic malformations. Neuropathol Appl Neurobiol. 2020;46(6):546-563.

51. Rettew JA, McCall SH, Marriott I. GPR30/GPER-1 mediates rapid decreases in TLR4 expression on murine macrophages. Mol Cell Endocrinol. 2010;328(1–2):87–92.

52. Ghosh M, Xu Y, Pearse DD. Cyclic AMP is a key regulator of M1 to M2a phenotypic conversion of microglia in the presence of Th2 cytokines. J Neuroinflammation. 2016;13:9.

53. Li C, Chen T, Zhou H, Feng Y, Hoi MPM, Ma D, et al. BHDPC is a novel neuroprotectant that provides anti-neuroinflammatory and neuroprotective effects by inactivating NF-kappaB and activating PKA/CREB. Front Pharmacol. 2018;9:614.

54. Mavi A, Cermik TF, Urhan M, Puskulcu H, Basu S, Yu JQ, et al. The effects of estrogen, progesterone, and C-erbB-2 receptor states on 18F-FDG uptake of primary breast cancer lesions. J Nucl Med. 2007;48(8):1266–72.

55. Zhao Z, Yoshida Y, Kurokawa T, Kiyono Y, Mori T, Okazawa H. 18F-FES and 18F-FDG PET for differential diagnosis and quantitative wvaluation of mesenchymal uterine tumors: Correlation with immunohistochemical analysis. J Nucl Med. 2013;54(4):499–506.

56. Barros RP, Gustafsson JA. Estrogen receptors and the metabolic network. Cell Metab. 2011;14(3):289–99.

57. Sharma G, Prossnitz ER. GPER/GPR30 knockout mice: effects of GPER on metabolism. Methods Mol Biol. 2016;1366:489–502.

58. Jin N, Qian W, Yin X, Zhang L, Iqbal K, Grundke-Iqbal I, et al. CREB regulates the expression of neuronal glucose transporter 3: a possible mechanism related to impaired brain glucose uptake in Alzheimer's disease. Nucleic Acids Res. 2013;41(5):3240–56.

59. Yang L. Neuronal cAMP/PKA signaling and energy homeostasis. Adv Exp Med Biol. 2018;1090:31–48.

60. Wang A, Luo J, Moore W, Alkhalidy H, Wu L, Zhang J, et al. GPR30 regulates diet-induced adiposity in female mice and adipogenesis in vitro. Sci Rep. 2016;6:34302.

61. Sharma G, Prossnitz ER. G-protein-coupled estrogen receptor (GPER) and sex-specific metabolic homeostasis. Adv Exp Med Biol. 2017;1043:427–53.

62. Cotter JA. An update on the central nervous system manifestations of tuberous sclerosis complex. Acta Neuropathol. 2020;139(4):613–24.

63. Lu DS, Karas PJ, Krueger DA, Weiner HL. Central nervous system manifestations of tuberous sclerosis complex. Am J Med Genet C Semin Med Genet. 2018;178(3):291–8.

SUPPORTING INFORMATION

Additional supporting information may be found online in the Supporting Information section.

FIGURE S1 Relative localization of GFAP, Vimentin, and SMI32 in DNs (black arrows) and BCs (red arrows) of the patients with FCDIIb and TSC. (A, D) Immunostaining of GFAP. BCs are immunoreactive for GFAP, and no immunoreactivity for GFAP was found in DNs. (B, E) Immunostaining of vimentin. BCs are immunoreactive for Vimentin, and no immunoreactivity for Vimentin was found in DNs. (C, F) Immunostaining of SMI32. Both DNs and BCs are immunoreactive for SMI32. Scare bars: 50 μm

FIGURE S2 Evaluation of GPR30, PKA, p-PKA, and NF-κB immunostaining in DNs (black arrows) and BCs (red arrows) of the specimens of female patients with FCDIIb and TSC. (A, E) Immunostaining of GPR30. Both DNs and BCs are immunoreactive for GPR30. (B, F) Immunostaining of PKA. Both DNs and BCs are immunoreactive for PKA. (C, G) Immunostaining of p-PKA. Both DNs and BCs are immunoreactive for p-PKA. (D, H) Immunostaining of NF-κB. Both DNs and BCs are immunoreactive for NF-κB. Scare bars: 50 μm. (I) The immunoreactive score of GPR30, PKA, p-PKA, and NF-κB in DNs and BCs of female patients with FCDIIb. (J) The immunoreactive score of GPR30, PKA, p-PKA, and NF-κB in DNs and BCs of female patients with TSC

FIGURE S3 Correlation analysis between GPR30 and the SUVs in total and male patients with FCDIIb and TSC. (A) The axial (A_1) and coronal (A_2) PET-CT images of patients with FCDIIb. Red circles were used to

mark the epileptogenic foci of patients with FCDIIb. (B, C) Correlation of GPR30 with the SUVs (SUVmax and SUVmean) in total patients with FCDIIb. There were no significant correlations of GPR30 with SUVmax and SUVmean (r = 0.3123, p = 0.1373; r = 0.3059 p = 0.1461). (D, E) Correlation of GPR30 with the SUVs in the male patients with FCDIIb. No significant correlations were found (SUVmax: r = 0.2898, p = 0.4494; SUVmean: r = 0.04364 p = 0.9112). (F) The axial (F_1) and coronal (F_2) PET images of patients with TSC. Red circles were used to mark the epileptogenic foci of patients with TSC. (G, H) Correlation of GPR30 with the SUVs in total patients with TSC. No significant correlations of GPR30 with SUVmax and SUVmean were found (r = 0.3033, p = 0.1321; r = 0.1752 p = 0.3921). (I, J) Correlation of GPR30 with the SUVs in the male patients with TSC. SUVmax and SUVmean were not correlated with the expression of GPR30 (r = −0.6096, p = 0.1086; r = −0.2652, p = 0.5255)

FIGURE S4 Spearman's rank correlation test of GPR30 and SUVs in the non-epileptogenic tubers. (A, B) No correlation of GPR30 with SUVmax (r = 0.3633, p = 0.2225) or SUVmean (r = 0.4130, p = 0.1607) was found in the non-epileptogenic tubers